CrystEngComm

ROYAL SOCIETY OF CHEMISTRY

COMMUNICATION

View Article Online
View Journal | View Issue

Cite this: *CrystEngComm*, 2025, **27**, 5788

Received 5th July 2025,
Accepted 1st August 2025

DOI: 10.1039/d5ce00674k

rsc.li/crystengcomm

A highly hydrogen-bonded {Cu_2Co} cyanide complex exhibiting high room-temperature proton conduction

Qi-Juan Cai,†[a] Lu-Yao Ma,†[a] Kun-Hua Zhang,[a] Fu-Wan Dong,[a] Ao-Na Sun,[a] Jiong Yang[b] and Dong Shao *[a]

A trinuclear cyanide-bridged {Cu_2Co} complex featuring a highly hydrogen-bonded 3D supramolecular structure was structurally, magnetically, and electrically characterized. Alternating current (AC) impedance measurements indicate that the complex exhibits temperature- and humidity-dependent proton conduction behavior with a superionic conductivity of around 10^{-3} S cm^{-1} at room temperature. The high conductivity is attributed to strongly (N–H···O and O–H···O) hydrogen-bonded 1D protonic water chains within the supramolecular framework.

Proton-conducting materials have garnered increasing attention in recent years due to their broad application prospects in electrochemical devices such as fuel cells and battery systems.[1–3] To date, a variety of solid-state proton conductors, including polymers, ceramic oxides, and oxoacids, have been extensively investigated. Additionally, significant progress has been made in the development of molecular-based proton conductors, with many molecular materials demonstrating excellent proton conductivity over a wide temperature range. Among these, hydrogen-bonded supramolecular systems, including hydrogen-bonded organic frameworks (HOFs), metallo HOFs, and organic cages, have emerged as prominent research focuses due to their high crystallinity, tunable supramolecular structures, flexible designability, and potential for functionalization.[4–13] Recent advancements in proton-conducting molecular materials have enabled them to rival or even surpass traditional electrolyte materials (*e.g.*, Nafion) in terms of high proton conductivity and stability.[14] The core mechanism of proton conduction relies heavily on efficient proton migration pathways, with hydrogen-bonding networks playing a critical role in this process.[15] Specifically, proton conduction mechanisms primarily include two types: proton hopping through dense hydrogen-bonding networks (Grotthuss mechanism) and proton transport through diffusion channels filled with discrete hydrogen-bonded clusters (vehicle mechanism). To optimize these conduction pathways, the incorporation of guest molecules (*e.g.*, water molecules) to form specific proton-conducting channels has proven to be an effective strategy.[16–21] Consequently, the design of molecular materials with one-dimensional (1D) protonic water chains has become a highly attractive strategy for achieving efficient proton transport; however, it remains difficult to build such a unique structure in a designed way.[22]

Cyanide-bridged coordination compounds, as an important class of molecular magnetic materials, have attracted considerable attention due to their unique magnetic properties and tunable hydrogen-bonded characteristics.[23–26] These materials are assembled from cyanometallates, ligands, and metal ions or complex building blocks, exhibiting not only rich magnetic behaviors, such as magnetic ordering, single-ion magnets, and spin crossover, but also notable hydrogen bonding interactions.[27–30] Recently, proton conduction has been observed in several cyanide-bridged framework materials.[31–36] For instance, Ohtani and colleagues observed a strong correlation between the polar skeleton and conducting protons in K_2-$MnN(CN)_4{\cdot}H_2O$, which showed anomalous ferroelectricity and proton conductivity. This observation highlights the potential application of cyanide-bridged materials in the field of proton conduction.

Herein, we report the synthesis, structure, and magnetic and electrical characterization of a trinuclear cyanide-bridged cluster molecule, $(H_3O)\{[Co^{III}(CN)_6][Cu^{II}(cyclam)]_2\}[[Co^{III}(CN)_6]]{\cdot}5H_2O$ (cyclam = 1,4,8,11-tetraazacyclotetradecane, Fig. 1), based on diamagnetic hexacyanidocobaltate(III). Structural analysis reveals notable

[a] *Hubei Key Laboratory of Processing and Application of Catalytic Materials, Hubei Provincial Engineering Research Center of High Purity Raw Material Processing Technology of Electronic Materials, College of Chemistry and Chemical Engineering, Huanggang Normal University, Huanggang 438000, China. E-mail: shaodong@nju.edu.cn*

[b] *Department of Chemistry, Southern University of Science and Technology, Shenzhen 518055, China*

† Q. J. C. and L. Y. M. contributed equally to this paper.

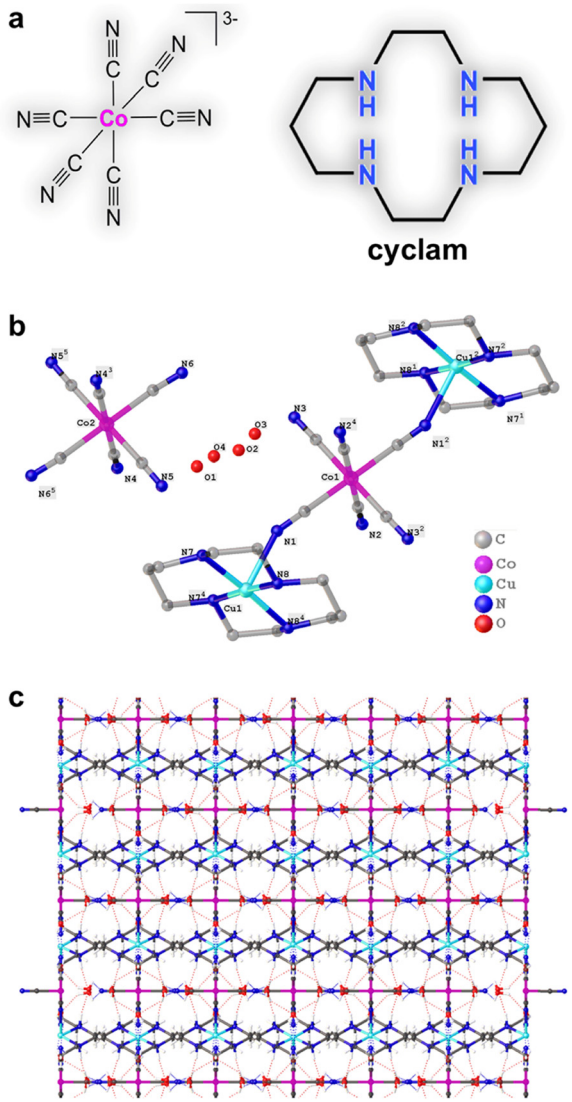

Fig. 1 (a) Molecular structures of the used $[Co^{III}(CN)_6]^{3-}$ and cyclam ligand. (b) Crystal structure of **1**. (c) Packing hydrogen-bonded supramolecular structure of **1** viewed along the *c* axis.

hydrogen-bonded networks sustained by charge-assisted hydrogen-bonds between $[Co^{III}(CN)_6]^{3-}$, guest water, and H_3O^+, and trinuclear $\{Cu_2Co\}$ units. Interestingly, 1D hydrogen-bonded water chains were formed within the material, leading to the observation of temperature- and humidity-dependent proton conduction even at room temperature, indicating that the compound is a good proton conductor.

Single-crystal X-ray results revealed a monoclinic *C*2/*m* space group (Table S1). In the asymmetric unit, one half $\{[Co^{III}(CN)_6][Cu^{II}(cyclam)]\}$ unit, one half $[Co(CN)_6]^{3-}$ as a counter anion, and four water molecules can be found (Fig. S1). Among the water molecules, one of them (O2) is protonated to achieve charge balance. By the symmetry code, the complete molecule is a trinuclear structure (Fig. 1), in which two $[Cu^{II}(cyclam)]$ units featuring a five-coordinated geometry are bridged by one $[Co(CN)_6]^{3-}$. Coincidentally, the isolated $[Co(CN)_6]^{3-}$ units are located in the center of two neighboring $\{[Co^{III}(CN)_6][Cu^{II}(cyclam)]_2\}$ units with a distance of 3.611 Å between terminal cyano N from $[Co(CN)_6]^{3-}$ and the Cu^{2+} ion. This long distance prevents the formation of a 1D chain complex. Selected bond lengths (Å) and angles are summarized in Tables S1 and S2. The average Cu–N and Co–C bond lengths are 2.077(7) and 1.891(2) Å (Table S2), respectively, supporting a high-spin Cu^{2+} ion and a low spin Co^{3+} ion. Continuous shape measure (CShM) analysis indicates that the Co^{3+} ion is located in a near-perfect octahedral geometry while the Cu^{2+} ions are in a distorted square pyramidal geometry with the parameter being 0.867 (Table S4). The potential hydrogen bonds were determined using PLATON (Table S5). The guest water molecule connects along the *a* direction *via* multiple and short O–H···O hydrogen bonds (O4···H1A–O1, 2.011 Å; O1···H3B–O3, 1.962 Å; O3···H2B–O2, 1.954 Å), forming unique 1D hydrogen-bonded water chains (Fig. S2). The water molecules also form OH···N and NH···O hydrogen bonds with neighboring terminal cyano N and N–H from cyclam ligands, finally giving rise to a highly H-bonded 3D network (Fig. 1c and S3). In addition, the packing diagrams show that the Cu^{2+} ions are well isolated from one another, with the shortest intermolecular $Cu^{2+}\cdots Cu^{2+}$ distances being 9.650 Å.

Powder X-ray diffraction (PXRD) analysis was conducted on the bulk crystalline sample of compound **1** before the measurements (Fig. S4). The experimental pattern demonstrated high phase purity, as evidenced by the close agreement between the simulated and experimental patterns. Thermal gravimetric analysis revealed that the material remains stable below 60 °C (Fig. S5), followed by the gradual loss of lattice water molecules as the temperature increased from 60 to approximately 130 °C. The observed weight loss of 18.5% closely matched the calculated value of 18.32% based on crystallographic data. Subsequent heating to around 280 °C after the removal of all water molecules did not result in any further experimental weight loss.

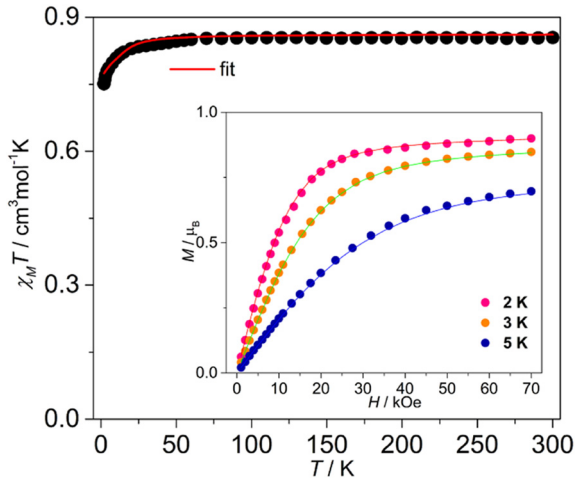

Fig. 2 $\chi_M T$ *vs.* *T* plots for **1** at 1 kOe. Inset: *M* *vs.* *H* plots for **1**. Solid curves are fitted results *via* PHI.

To further probe the magnetic properties of complex **1**, direct current (dc) magnetic susceptibility measurements were performed on well-ground crystals of **1** (Fig. 2). Structural analysis indicates that the paramagnetic Cu(II) ions are well separated by diamagnetic $[Co^{III}(CN)_6]^{3-}$ bridges. Consequently, the trinuclear cluster behaves magnetically as an isolated single-ion system. At 300 K, the $\chi_M T$ value for **1** is 0.854 $cm^3\ mol^{-1}$ K, slightly exceeding the spin-only value of 0.75 $cm^3\ mol^{-1}$ K expected for two uncoupled Cu^{2+} ions (S = 1/2, g = 2.0). This deviation suggests small zero-field splitting (ZFS) in the distorted octahedral Cu^{2+} centers.[37–39] The $\chi_M T$ product remains nearly constant down to approximately 20 K, below which it decreases sharply to a minimum of 0.725 $cm^3\ mol^{-1}$ K. Additionally, variable-field magnetization measurements were conducted at different temperatures (Fig. 3, inset). The magnetization value at 2 K and 7 T is 1.817 μ_B, which is lower than the saturation value expected for two uncoupled high-spin Cu^{2+} ions. This observation is consistent with the presence of ZFS in the Cu^{2+} ions. To obtain the ZSF parameters, the magnetic susceptibility and magnetization data were fitted *via* the PHI program. The best fit gives D = −1.03 cm^{-1}, and g_x = 2.013, g_y = 2.008, and g_z = 2.170, indicative of negligible magnetic anisotropy. Furthermore, ac susceptibility measurement was performed on **1** (Fig. S6), but the χ'' signals did not show any slow relaxation of the magnetization behaviour, even when external fields were applied.

The unique structural features of **1** (Fig. S7 and S4a), including directional hydrogen-bonded water chains, lattice water molecules, and proton carriers (H_3O^+), prompted us to investigate its proton conduction properties. Alternating current (AC) impedance spectroscopy was employed to measure the proton conductivity of **1** at 30 °C under varying relative humidity (RH) conditions. The Nyquist plot (Fig. 3a) exhibited a characteristic semicircle in the high-frequency region and a capacitive tail at low frequencies, confirming proton conduction behavior.[40–46] The bulk conductivity was derived from semicircle fitting of the impedance data (Table S6). Notably, the conductivity of **1** exhibited a nonlinear increase with rising RH (Fig. 3b), progressing from 6.6×10^{-8} S cm^{-1} (25 °C, 45% RH) to 1.3×10^{-3} S cm^{-1} (95% RH). This enhancement is attributed to the increased water adsorption at higher humidity, which facilitates proton carrier diffusion. The high conductivity observed at room temperature suggests that **1** behaves as a good superprotonic conductor, which is comparable to those of benchmark proton-conducting crystalline materials in which proton conductivity has been tested under similar experimental conditions, for example, MFM-500(Ni) (4.5×10^{-4} S cm^{-1}),[47] MOF-74(Ni) (5.3×10^{-5} S cm^{-1}),[48] CB[6]·1.2·H_2SO_4·6.4H_2O (1.3×10^{-3} S cm^{-1}),[49] and Fe(ox)·2H_2O (1.3×10^{-3} S cm^{-1}).[50]

Temperature-dependent studies (40–90 °C) further revealed a strong thermal activation effect on proton transport. The conductivity increased significantly from 2.1×10^{-3} S cm^{-1} at 30 °C to 3.1×10^{-2} S cm^{-1} at 90 °C under 95% RH (Fig. 3c and Table S7), representing a fifteen-fold enhancement. This trend is consistent with thermally accelerated proton migration, where elevated temperatures promote both water mobility and the formation of H_3O^+ as proton carriers. The proton conductivity of **1** compares favorably with other cyanide-based proton conductors.[31–36] Post-measurement PXRD analysis (Fig. S8) confirmed that the framework remained structurally intact after humidity and temperature cycling, underscoring its stability under operational conditions.

To elucidate the proton conduction mechanism of **1**, we analyzed the temperature-dependent conductivity data using the Arrhenius equation: $\sigma T = \sigma_0 \exp(E_a/k_B T)$. The fitted curve yielded an activation energy (E_a) of 0.36 eV for **1** (Fig. 3d), providing insight into the proton transport process. Proton conduction typically occurs *via* two distinct mechanisms: 1) the Grotthuss mechanism, where protons hop through hydrogen-bonded water networks or ordered pathways, characterized by a low E_a range (0.1–0.4 eV), and 2) the vehicle mechanism, where protons diffuse *via* the directional migration of hydrated carriers (*e.g.*, H_3O^+), requiring higher energy ($E_a > 0.4$ eV). The observed E_a value (0.36 eV) indicates that proton conduction in **1** follows the Grotthuss mechanism. This is facilitated by a continuous hydrogen-bonding network between the {Cu_2Co} clusters and lattice water molecules, enabling efficient proton hopping. Furthermore, prior studies suggested that frameworks stabilized by charge-balancing counter-cations often exhibit enhanced proton conductivity, aligning with the superior performance observed for **1**. The proton migration pathways, depicted in Fig. 4b, are formed by 1D continuous hydrogen-bonded water chains. It is postulated that protons originating from cyclam and/or H_3O^+ transfer among the water molecules *via* hydrogen-bonding chains, facilitating swift and effective H^+ migration.

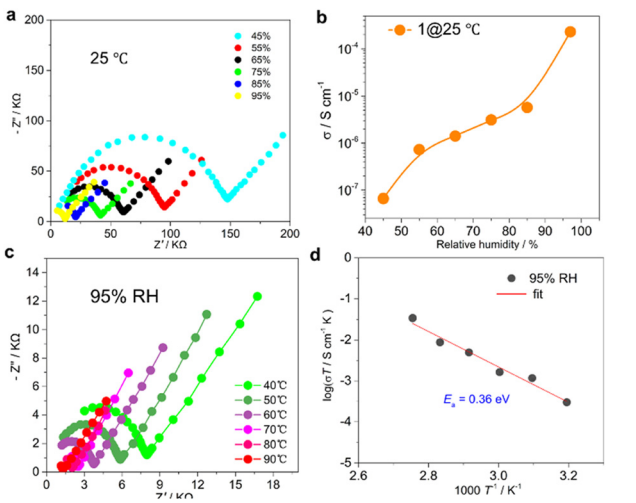

Fig. 3 (a) Nyquist diagrams of **1** under 75–95% RH at 25 °C. (b) The trend diagram of σ with RH at a fixed temperature of 30 °C. (c) Nyquist plots of **1** under 95% RH at 55–97 °C. (d) Arrhenius plots and linear fitting of temperature-dependent conductivity at 95% RH of **1**.

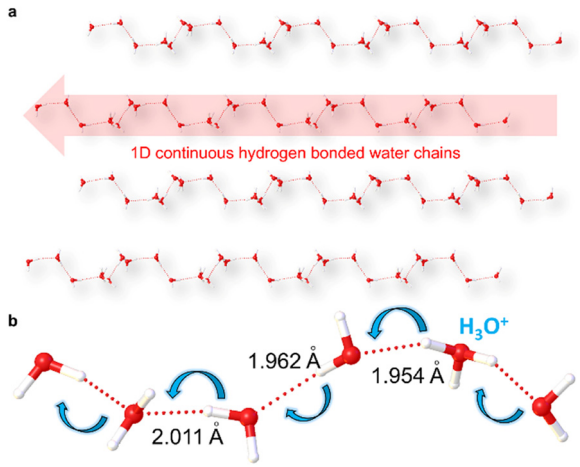

Fig. 4 (a) 1D continuous hydrogen bonding water chains in **1**. (b) Possible proton migration pathways of **1**.

The recyclability and stability of proton conductors are critical for their practical applications. To evaluate these properties for **1**, we conducted systematic temperature-cycling experiments. The proton conductivity values obtained during the heating and cooling cycles exhibited excellent consistency (Fig. S9), demonstrating remarkable repeatability and thermal stability. To assess long-term stability, we performed time-dependent conductivity measurements at 25 °C and 95% RH over 10 hours. As illustrated in Fig. S10, the proton conductivity of **1** showed negligible degradation, underscoring its exceptional operational durability. These results collectively highlight the robustness of **1** as a promising proton-conducting material for practical applications.

In summary, we reported the synthesis and structural, magnetic, and electrical properties of a cyanide-bridged trinuclear {Cu_2Co} complex constructed from diamagnetic hexacyanidocobaltate(III) and paramagnetic $[Cu(cyclam)]^{2+}$ units. Structural analysis indicates a highly hydrogen-bonded 3D supramolecular structure sustained by multiple N–H···O and O–H···O hydrogen bonds. Notably, hydrogen-bonded 1D protonic water chains were formed in the structure, providing a unique proton transport pathway. AC impedance measurements indicate that the complex exhibits temperature- and humidity-dependent proton conduction behavior with a superionic conductivity of around 10^{-3} S cm^{-1} at room temperature. This work not only provides a good cyanide-based magnetic proton-conducting material but also highlights the rational design of hydrogen-bonded supramolecular structures through a cyanometallate strategy.

Conflicts of interest

There are no conflicts to declare.

Data availability

Supplementary Information available: Experimental details, physical measurements, crystallographic data, CShM calculated results, PXRD pattern, and additional Nyquist plots. See DOI: **https://doi.org/10.1039/D5CE00674K**.

CCDC 2431134 contains the supplementary crystallographic data for this paper.[51]

Acknowledgements

We acknowledge the Chutian Scholars Program of Hubei Province, Huanggang Normal University (2042021033, 202210204), and the Hubei Province Natural Science Foundation (2023AFB010, 2025AFD359).

Notes and references

1 K.-D. Kreuer, S. J. Paddison, E. Spohr and M. Schuster, *Chem. Rev.*, 2004, **104**, 4637–4678.
2 P. Colomban, *Proton Conductors: Solids, Membranes and Gels – Materials and Devices*, Cambridge University Press, Cambridge, 1992.
3 S. C. Pal and M. C. Das, *Adv. Funct. Mater.*, 2021, **31**, 2101584.
4 S. C. Pal, D. Mukherjee, Y. Oruganti, B. G. Lee, D.-W. Lim, B. Pramanik, A. K. Manna and M. C. Das, *J. Am. Chem. Soc.*, 2024, **146**, 14546–14557.
5 S. C. Pal, D. Mukherjee, R. Sahoo, S. Mondal and M. C. Das, *ACS Energy Lett.*, 2021, **6**, 4431–4453.
6 Z. Wang, L. Yang, Q. Chen, P. Liu, Z. Yang, H. Li, X. Huang and W. Huang, *Adv. Mater.*, 2024, **36**, 2409202.
7 S. Chand, Z. Zhang, S. C. Pal, A. Pal, Y. Ye, Q. Lin, S. Xiang and M. C. Das, *Chem. – Eur. J.*, 2019, **25**, 1691–1695.
8 Y. Qin, T. Gao, W.-P. Xie, Z. Li and G. Li, *ACS Appl. Mater. Interfaces*, 2019, **11**, 31018–31027.
9 Q.-X. Wang, Z.-C. Guo, Y. Qin, X. Wang and G. Li, *Inorg. Chem.*, 2021, **60**, 19278–19286.
10 D. Shao, Y. Zhou, X. Yang, J. Yue, S. Ming, X.-Q. Wei and Z. Tian, *Dalton Trans.*, 2022, **51**, 18514–18519.
11 D. Shao, L. Shi, G. Liu, J. Yue, S. Ming, X. Yang, J. Zhu and Z. Ruan, *Cryst. Growth Des.*, 2023, **23**, 5035–5042.
12 J. Dong, L. Huang, L. Shi, J. Yang, Y. Wan and D. Shao, *Inorg. Chem.*, 2024, **63**, 17478–17487.
13 S.-J. Chen, B. Yao, Y. Chen, F.-W. Dong, J. Yang, L. Huang and D. Shao, *Inorg. Chem.*, 2025, **64**, 4141–4150.
14 S. C. Pal and M. C. Das, *Adv. Funct. Mater.*, 2021, **31**, 2101584.
15 D. Mukherjee, A. Saha, S. Moni, D. Volkmer and M. C. Das, *J. Am. Chem. Soc.*, 2025, **147**, 5515–5553.
16 R. Saha and C. J. G. García, *Chem. Soc. Rev.*, 2024, **53**, 9490–9559.
17 K. Otsubo, S. Nagayama, S. Kawaguchi, K. Sugimoto and H. Kitagawa, *JACS Au*, 2022, **2**, 109–115.
18 S. Chand, S. C. Pal, D.-W. Lim, K. Otsubo, A. Pal, H. Kitagawa and M. C. Das, *ACS Mater. Lett.*, 2020, **2**, 1343–1350.
19 G. Wang, C. Zhao, Y. Lu, J. Yang, X. Bai, Y. Yang, M. Zhu, C. Geng and S. Liu, *Inorg. Chem.*, 2025, **64**, 12331–12341.

20 M. O'Shaughnessy, J. Lim, J. Glover, A. R. Neale, G. M. Day, L. J. Hardwick and A. I. Cooper, *J. Am. Chem. Soc.*, 2025, **147**, 15429–15434.
21 F. Yang, G. Xu, Y. Dou, B. Wang, H. Zhang, H. Wu, W. Zhou, J.-R. Li and B. Chen, *Nat. Energy*, 2017, **2**, 877–883.
22 K. Otake, K. Otsubo, T. Komatsu, S. Dekura, J. M. Taylor, R. Ikeda, K. Sugimoto, A. Fujiwara, C.-P. Chou, A. W. Sakti, Y. Nishimura, H. Nakai and H. Kitagawa, *Nat. Chem.*, 2020, **11**, 843–850.
23 J. Yadav, R. Kharel and S. Konar, *Coord. Chem. Rev.*, 2025, **523**, 216283.
24 Z.-Y. Chen, Q. Liu, Y. Cheng, Y.-F. Deng, S. Liu, X.-Y. Wang and Y.-Z. Zhang, *Angew. Chem., Int. Ed.*, 2023, **62**, e202301124.
25 X.-H. Zhao, D. Shao, J.-T. Chen, D.-X. Gan, J. Yang and Y.-Z. Zhang, *Sci. China:Chem.*, 2022, **65**, 532–538.
26 L. Shi, D. Shao, X.-Q. Wei, K. R. Dunbar and X.-Y. Wang, *Angew. Chem., Int. Ed.*, 2020, **59**, 10379–10384.
27 M. You, D. Shao, Y.-F. Deng, J. Yang, N.-T. Yao, Y.-S. Meng, L. Ungur and Y.-Z. Zhang, *Inorg. Chem.*, 2022, **61**, 5855–5860.
28 D. Shao, Y. Zhou, Q. Pi, F.-X. Shen, S.-R. Yang, S.-L. Zhang and X.-Y. Wang, *Dalton Trans.*, 2017, **46**, 9088–9096.
29 F.-X. Xu, Y.-L. Li, X.-Q. Wei, D. Shao, L. Shi, H.-Y. Wei and X.-Y. Wang, *Dalton Trans.*, 2023, **52**, 5575–5586.
30 L. Shi, J. Kobylarczyk, K. Dziedzic-Kocurek, J. J. Stanek, B. Sieklucka and R. Podgajny, *Inorg. Chem.*, 2023, **62**, 7032–7044.
31 Y. Shi, S. Kimura, Y. Iwai, Y. Tsuji, B. Le Ouay, M. Ohba and R. Ohtani, *Inorg. Chem.*, 2024, **63**, 22194–22202.
32 M. Reczyński, M. Pazera and M. Magott, *Inorg. Chem.*, 2025, **64**, 7397–7406.
33 J. Wang, J. J. Zakrzewski, M. Heczko, M. Zychowicz, K. Nakagawa, K. Nakabayashi, B. Sieklucka, S. Chorazy and S. Ohkoshi, *J. Am. Chem. Soc.*, 2020, **142**, 3970–3979.
34 J. Yanagisawa, T. Aoyama, K. Fujii, M. Yashima, Y. Inaguma, A. Kuwabara, K. Shitara, B. Le Ouay, S. Hayami, M. Ohba and R. Ohtani, *J. Am. Chem. Soc.*, 2024, **146**, 1476–1483.
35 Y. Zhou, H. Xiang, J.-Y. Zhu, L. Shi, W.-J. You, X.-Q. Wei, Z. Tian and D. Shao, *Polyhedron*, 2022, **228**, 116181.
36 Y. Song, Y. Tsuji, K. Sugimoto, T. Kikuchi, Y. Shi, Y. Murakami, K. Hiramatsu, B. Le Ouay, M. Ohba and R. Ohtani, *Chem. Sci.*, 2025, **16**, 13413–13421.
37 H. Kato, Y. Horii, M. Noguchi, T. Kajiwara and H. Fujimori, *Chem. Commun.*, 2023, **59**, 14587–14590.
38 R. Boča, C. Rajnák, J. Titiš and D. Valigura, *Inorg. Chem.*, 2017, **56**, 1478–1482.
39 E. Pilichos, M. Font-Bardia, A. Escuer and J. Mayans, *Dalton Trans.*, 2022, **51**, 17653–17663.
40 Q. Wu, Q. Li, W. Zou, Z. Zhang, Y. Zhou and Q. Zhao, *Chem. Commun.*, 2025, **61**, 1842–1845.
41 R. Saha, A. Sharma, A. I. Siddiqui, S. Benmansour, J. Ortega-Castro, A. Frontera, B. Mondal, M. S. Lah and C. J. Gomez García, *Chem. Sci.*, 2025, **16**, 9501–9508.
42 J. J. Hu, K. L. Xie, T. Z. Xiong, M. M. Wang, H. R. Wen, Y. Peng and S. J. Liu, *Inorg. Chem.*, 2023, **62**, 12001–12008.
43 X. N. Zhang, B. C. Chen, J. L. Zhang, J. L. Zhang, S. J. Liu and H. R. Wen, *Dalton Trans.*, 2022, **51**, 15762–15770.
44 M. M. Wang, T. Z. Xiong, B. C. Chen, J. J. Hu, H. R. Wen and S. J. Liu, *Inorg. Chem.*, 2023, **62**, 21322–21328.
45 K. Wang, Z. Y. Li, Y. Peng, T. F. Zheng, J. L. Chen, S. J. Liu and H. R. Wen, *Inorg. Chem.*, 2023, **62**, 17993–18001.
46 Z. Y. Chen, J. Zhong, L. Wang, S. M. Song, H. Liu, T. F. Zheng, S. L. Yao and S. J. Liu, *J. Mol. Struct.*, 2024, **1300**, 137156.
47 S. Pili, S. P. Argent, C. G. Morris, P. Rought, V. Garcia-Sakai, I. P. Silverwood, T. L. Easun, M. Li, M. R. Warren, C. A. Murray, C. C. Tang, S. Yang and M. Schröder, *J. Am. Chem. Soc.*, 2016, **138**, 6352–6355.
48 W. J. Phang, W. R. Lee, K. Yoo, D. W. Ryu, B. Kim and C. S. Hong, *Angew. Chem., Int. Ed.*, 2014, **53**, 8383–8387.
49 M. Yoon, K. Suh, H. Kim, Y. Kim, N. Selvapalam and K. Kim, *Angew. Chem., Int. Ed.*, 2011, **50**, 7870–7873.
50 T. Yamada, M. Sadakiyo and H. Kitagawa, *J. Am. Chem. Soc.*, 2009, **131**, 3144–3145.
51 Q. J. Cai, L.-Y. Ma, K.-H. Zhang, F.-W. Dong, A.-N. Sun, J. Yang and D. Shao, 2025, DOI: **10.5517/ccdc.csd.cc2mlspq**.

